Mon. Not. R. Astron. Soc. **391,** 1961–1972 (2008) doi:10.1111/j.1365-2966.2008.14031.x

Fluctuations in the high-redshift Lyman–Werner background: close halo pairs as the origin of supermassive black holes

Mark Dijkstra,[1⋆] Zoltán Haiman,[2] Andrei Mesinger[3,4]† and J. Stuart B. Wyithe[5]

[1]*Astronomy Department, Harvard University, 60 Garden Street, Cambridge, MA 02138, USA*
[2]*Astronomy Department, Columbia University, 550 West 120th Street, New York, NY 10027, USA*
[3]*Department of Physics and Astronomy, UCLA, Los Angeles, CA 90095-1562, USA*
[4]*Department of Astrophysical Sciences, Princeton University, Princeton, NJ 08544, USA*
[5]*School of Physics, University of Melbourne, Parkville, Victoria 3010, Australia*

Accepted 2008 September 30. Received 2008 September 29; in original form 2008 July 30

ABSTRACT

The earliest generation of stars and black holes must have established an early 'Lyman–Werner' background (LWB) at high redshift, prior to the epoch of reionization. Because of the long mean free path of photons with energies $h\nu < 13.6$ eV, the LWB was nearly uniform. However, some variation in the LWB is expected due to the discrete nature of the sources, and their highly clustered spatial distribution. In this paper, we compute the probability distribution function (PDF) of the LW flux that irradiates dark matter (DM) haloes collapsing at high redshift ($z \approx 10$). Our model accounts for (i) the clustering of DM haloes, (ii) Poisson fluctuations in the number of corresponding star-forming galaxies and (iii) scatter in the LW luminosity produced by haloes of a given mass (calibrated using local observations). We find that >99 per cent of the DM haloes are illuminated by an LW flux within a factor of 2 of the global mean value. However, a small fraction, $\sim 10^{-8}$ to 10^{-6}, of DM haloes with virial temperatures $T_{\rm vir} \gtrsim 10^4$ K have a close luminous neighbour within $\lesssim$10 kpc, and are exposed to an LW flux exceeding the global mean by a factor of >20, or to $J_{21,\rm LW} > 10^3$ (in units of 10^{-21} erg s^{-1} Hz^{-1} sr^{-1} cm^{-2}). This large LW flux can photodissociate H_2 molecules in the gas collapsing due to atomic cooling in these haloes, and prevent its further cooling and fragmentation. Such close halo pairs therefore provide possible sites in which primordial gas clouds collapse directly into massive black holes ($M_{\rm BH} \approx 10^{4-6}\,{\rm M}_\odot$), and subsequently grow into supermassive ($M_{\rm BH} \gtrsim 10^9\,{\rm M}_\odot$) black holes by $z \approx 6$.

Key words: galaxies: high-redshift – quasars: general – cosmology: theory.

1 INTRODUCTION

Radiative feedback plays an important role in the formation of stars, black holes (BHs) and galaxies. Ionization and heating by photons with energies exceeding the hydrogen ionization threshold $E > E_{\rm H}$ affect the ability of gas to cool and collapse into dense objects (e.g. Couchman & Rees 1986; Efstathiou 1992; Thoul & Weinberg 1996; Kitayama & Ikeuchi 2000; Dijkstra et al. 2004). At the earliest epochs of structure formation, the dominant coolant of primordial gas clouds at gas temperatures $T \lesssim 10^4$ K are H_2 molecules (e.g. Saslaw & Zipoy 1967; Lepp & Shull 1984; Haiman, Thoul & Loeb 1996). The H_2 molecules can be photodissociated by ultraviolet (UV) radiation, either directly (by photons with energies $E > 14.7$ eV, if the molecules are exposed to ionizing radiation) or as a result of electronic excitation by Lyman–Werner (hereafter LW) photons with energies $11.2\,{\rm eV} \lesssim E < E_{\rm H}$. In this paper we focus on this latter process, which operates even in gas that is self-shielded, and/or in gas that is shielded by a neutral intergalactic medium (IGM) prior to the completion of reionization (see Haiman, Rees & Loeb 1997), from radiation at $E > E_{\rm H}$.

Photodissociation feedback possibly plays an important role in the formation of the supermassive black holes (SMBHs; $M_{\rm BH} \sim 10^9\,{\rm M}_\odot$) that existed at redshift $z > 6$, when the age of the Universe was <1 Gyr (e.g. Fan 2006). Several studies have modelled the growth of these SMBHs due to accretion and mergers, starting from stellar mass seed BHs left behind by the first generation of stars (e.g. Haiman & Loeb 2001; Bromley, Somerville & Fabian 2004; Haiman 2004; Yoo & Miralda-Escudé 2004; Shapiro 2005; Volonteri & Rees 2006; Johnson & Bromm 2007; Li et al. 2007; Tanaka & Haiman 2008). The generic conclusion is that it is challenging to account for the presence of several $\times 10^9\,{\rm M}_\odot$ SMBHs by $z \gtrsim 6$ if accretion is limited to the Eddington rate, unless the

⋆E-mail: mdijkstr@cfa.harvard.edu
†Hubble Fellow.

© 2008 The Authors. Journal compilation © 2008 RAS

Downloaded from https://academic.oup.com/mnras/article/391/4/1961/1747710 by Scuola Normale Superiore Biblioteca user on 12 December 2025

accretion is essentially uninterrupted over the Hubble time. Gravitational recoil during mergers can lead to the ejection of growing seed BHs from their parent haloes and can exacerbate the problem (Haiman 2004; Yoo & Miralda-Escudé 2004; Shapiro 2005; Volonteri & Rees 2006; Tanaka & Haiman 2008). An additional difficulty is that models successfully producing the several $\times 10^9$ $M_\odot$ SMBHs by $z \gtrsim 6$ tend to overproduce the number of lower mass BHs (Bromley et al. 2004; Tanaka & Haiman 2008).

Several alternative mechanisms have been proposed recently that evade these problems by having a period of rapid super-Eddington growth (e.g. Bromm & Loeb 2003; Volonteri & Rees 2005; Begelman, Volonteri & Rees 2006; Spaans & Silk 2006). The reason that photodissociation feedback may provide an interesting formation channel is that this feedback mechanism can affect gas cooling and collapse into haloes that have $T_{\rm vir} > 10^4$ K (e.g. Oh & Haiman 2002). Without H_2 molecules, gas inside these haloes collapses nearly isothermally due to atomic cooling, with the temperature remaining as high as $T \sim 10^4$ K, which may strongly suppress the ability of gas to fragment into stellar mass objects (e.g. Oh & Haiman 2002). Instead of fragmenting, this gas could rapidly accrete on to a seed BH (Volonteri & Rees 2005), or collapse directly into a very massive ($M_{\rm BH} = 10^4$–10^6 $M_\odot$) BH (Bromm & Loeb 2003; Begelman, Volonteri & Rees 2006; Lodato & Natarajan 2006; Spaans & Silk 2006; Lodato & Natarajan 2007; Volonteri, Lodato & Natarajan 2008), possibly with an intermediate state in the form of a very massive star (see Omukai, Schneider & Haiman 2008, for a more complete review). If these 'direct-collapse BHs' indeed formed, then they would provide a head start that could help explain the presence of SMBHs with inferred masses of several 10^9 $M_\odot$ per comoving Gpc^3 by $z \approx 6$.

Possibly the most stringent requirement for these rapid-growth models is the absence of H_2 molecules during cloud collapse. This requires the existence of a photodissociating background[1] whose mean intensity exceeds $J_{21,\rm LW} \geq J_{\rm crit} \sim 10^3$ (Bromm & Loeb 2003), where $J_{21,\rm LW}$ denotes the intensity in the LW background (in units of 10^{-21} erg s^{-1} Hz^{-1} sr^{-1} cm^{-2}, evaluated at the Lyman limit). Since LW photons propagate nearly unobscured through the high-redshift (neutral) IGM until they redshift into one of the Lyman series transitions of atomic hydrogen, each halo simultaneously 'sees' a large number of LW sources. Each halo is therefore expected to be exposed to approximately the same LW flux, close to the global mean level of the background, which is likely to be significantly lower than $J_{\rm crit}$ (Johnson, Greif & Bromm 2008; Omukai et al. 2008).

However, some variation in the LW flux that irradiates individual dark matter (DM) haloes is expected. For example, a DM halo with a nearby star-forming galaxy (separated e.g. by $d \approx 10$ kpc) will be exposed to an LW flux exceeding the global value, and reaching $J_{21,\rm LW} \sim 10^3 (d/10\,{\rm kpc})^{-2} [\dot{M}_*/(20\,M_\odot\,{\rm yr}^{-1})]$, where $\dot{M}_*$ is the star formation rate in the nearby galaxy (see Section 2.1.2 below for a more detailed discussion). In the present paper, we model this variation and compute the probability distribution function (PDF) of the LW flux that irradiates high-redshift DM haloes. In particular, we focus on the high-flux tail of this PDF, as our goal is to answer the following questions: what fraction of DM haloes with $T_{\rm vir} > 10^4$ K, collapsing at high redshift, are exposed to a flux exceeding $J_{\rm crit}$? Is this fraction sufficient to account for the space density of several $\times 10^9$ $M_\odot$ SMBHs at $z \approx 6$ inferred from observations?

In the model we present below, we account for the clustering of DM haloes. Proper modelling of clustering is important when one wants to model the high LW flux tail of the distribution, which is dominated by close pairs of haloes. We also account for Poisson fluctuations in the number of star-forming galaxies surrounding a halo, and allow for a scatter in LW luminosity produced in a halo with a given mass. In the local universe, the UV luminosity can vary by orders of magnitude for a given stellar mass (e.g. Schiminovich et al. 2007), and a similar variation of the UV luminosity is expected for a given total halo mass.

Spatial variations of the UV background have been investigated previously by several authors, especially in the context of the Lyman α forest at lower redshift. For example, Zuo (1992) studied the expected fluctuations in the *ionizing* radiation field produced by randomly distributed sources, and showed that the variance is significantly increased due to radiative transfer effects. More recently, Mesinger & Dijkstra (2008) studied the expected fluctuations of the ionizing background during the advanced stages of reionization using 'seminumerical' simulations. Previous works have studied various observable consequences of fluctuations in the ionizing background on the lower redshift ($z \lesssim 5.5$) Lyα forest (e.g. Croft 2004; Meiksin & White 2004; Schaye 2006). Existing work on the evolution of the LW background has focused on its global (volume averaged) build-up with time, and the impact on subsequent star formation (e.g. Haiman, Abel & Rees 2000; Mesinger, Bryan & Haiman 2006; Johnson et al. 2008). The main differences of our study from these earlier works are that (i) we include the non-linear clustering of sources, (ii) we specialize to compute the PDF of the flux as seen by high-redshift DM haloes, (iii) we allow the UV luminosity for a given halo mass to be variable, instead of assuming a rigid one-to-one correspondence between halo mass and UV luminosity, (iv) we focus on the tail of the flux PDF and (v) we discuss the significance of this tail for rapid high-redshift SMBH growth [note however that the work presented by Mesinger & Dijkstra (2008) did include effects (i) and (ii)]. While this paper was being completed, we became aware of related work by Ahn et al. (2008), who studied the inhomogeneity of the LW background with cosmological simulations. Their paper focuses mostly on the impact of these fluctuations on the star formation efficiency in minihaloes (as opposed to the tail of the PDF and its significance to SMBH formation, which is the focus of our study). The papers seem to agree wherever there is overlap: the $z = 10.5$ LW flux PDF shown in fig. 11 of Ahn et al. (2008) is consistent with our results (e.g. Fig. 2).

The outline of this paper is as follows: In Section 2, we describe our model for calculating the LW flux PDF. In Section 3, we present our results. Model uncertainties and the implications of our work are discussed in Section 4, before summarizing our main conclusions in Section 5. The parameters for the background cosmology used throughout this paper are $(\Omega_{\rm m}, \Omega_\Lambda, \Omega_{\rm b}, h, \sigma_8) = (0.27, 0.73, 0.042, 0.70, 0.82)$, consistent with 5-yr data from the *Wilkinson Microwave Anisotropy Probe* (*WMAP*) (Dunkley et al. 2008; Komatsu et al. 2008).

2 THE MODEL

This section, which describes our numerical modelling, is split into three parts. In Section 2.1, we describe how we model the non-linear spatial clustering of sources around the position of a DM halo. In Section 2.2, we describe how we generate a discrete number of UV

[1] Note that the gas could remain H_2-free and close to $T \sim 10^4$ K if its atomic cooling rate was reduced sufficiently due to the trapping of Lyman line radiation (Spaans & Silk 2006).

Downloaded from https://academic.oup.com/mnras/article/391/4/1961/1747710 by Scuola Normale Superiore Biblioteca user on 12 December 2025

sources from a continuous density field, and how we assign UV luminosities to individual sources by using a Monte Carlo (MC) technique. In Section 2.3, we discuss how we finally obtain the total intensity of the LW radiation field ($J_{\rm LW}$) that the halo is exposed to. This procedure yields individual realizations for $J_{\rm LW}$ seen by a single halo. A distribution for $J_{\rm LW}$ is obtained by performing multiple MC realizations for a range of halo masses.

2.1 Modelling the Lyman–Werner background as sampled by dark matter haloes

2.1.1 The clustering of sources around a halo

Consider a halo of total (DM + gas) mass M that virializes at redshift z. The average number $\mathcal{N}(m, r)\,{\rm d}m\,{\rm d}r$ of haloes within the mass range $m \pm {\rm d}m/2$ that populate a surrounding spherical shell of physical radius r and thickness ${\rm d}r$, is given by

$$\mathcal{N}(m, r)\,{\rm d}m\,{\rm d}r = 4\pi r^2\,{\rm d}r \times (1+z)^3 \frac{{\rm d}n_{\rm ST}(m, z)}{{\rm d}m}\,{\rm d}m[1 + \xi(M, m, z, r)]. \quad (1)$$

Here ${\rm d}n_{\rm ST}(m, z)/{\rm d}m$ is the Press–Schechter (1974) mass function (with the modification of Sheth, Mo & Tormen 2001), which gives the number density of haloes of mass m (in units of *comoving* Mpc^{-3}). The factor $(1 + z)^3$ converts the number density of haloes into proper Mpc^{-3}.

For simplicity, we assume a static Euclidean space in our calculations. Cosmological corrections affect only sources at distances comparable to the Hubble length from the central halo, and we have explicitly verified that the value of the global LW background would be changed by less than a factor of $\sim$2. Since this is within the uncertainty in the flux attenuation due to the uncertain intergalactic H_2 abundance (see Section 4.1), we have ignored these cosmological corrections throughout our paper for simplicity.

The quantity $\xi(M, m, z, r)$ denotes the two-point correlation function, which gives the excess (above random) probability of finding a halo of mass m at a distance r from the central halo. In this paper we are especially interested in the high-end tail of the PDF flux impinging upon haloes of mass M. Since, as we demonstrate below, this tail is dominated by close pairs of haloes, we would like to model the clustering of closely separated haloes as accurately as possible. To this end we use the analytic formulation of non-linear Eulerian bias developed by Iliev et al. (2003), which fits the two-point correlation function derived from N-body simulations significantly better than the standard linear-bias approximation (Mo & White 1996; Scannapieco & Barkana 2002), especially at small separations.

The benefit of using this non-linear bias formalism is illustrated in Fig. 1, where we show, as an example, the two-point correlation function $\xi(M, m, z, r)$ for $z = 10$, and $M = m = 1.7 \times 10^8\,{\rm M}_\odot$. Here, the solid (dashed) curve shows the non-linear (linear) bias approximation, while the histogram shows the two-point correlation function derived from a 'seminumerical' simulation (Mesinger & Furlanetto 2007). In this simulation, an excursion-set approach is combined with first-order Lagrangian perturbation theory to generate density, velocity and halo fields at $z = 10$ (for a more detailed description of this approach, the reader is referred to Mesinger & Furlanetto 2007). The simulation does not resolve scales below $r \sim 0.14$ Mpc. Clearly, the non-linear bias formalism matches the simulation much better, especially at $r < 1$ (comoving) Mpc. Furthermore, Fig. 1 shows that in the range of $r \approx$ 10–100 (comoving) kpc, the two-point function in the non-linear case exceeds the linear-bias prediction by one to two orders of magnitude. Recently, Hennawi et al. (2006) have found a large excess of close quasar pairs, which implies a steepening of the (projected) two-point correlation function, which is perhaps an observational signature of non-linear clustering.

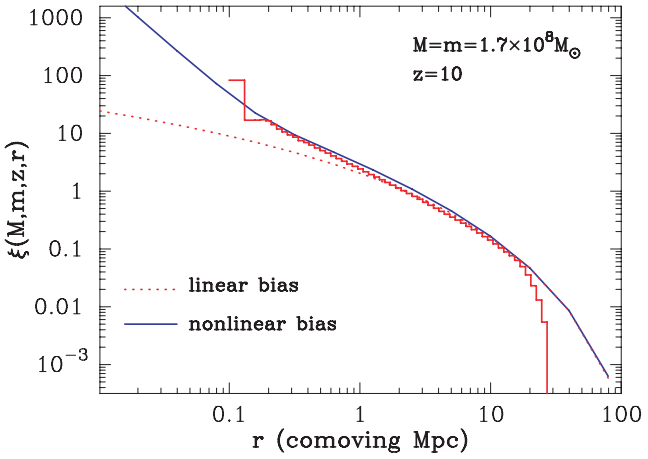

Figure 1. The two-point correlation function $\xi(M, m, z, r)$ is shown for redshift $z = 10$, and halo masses $M = m = 1.7 \times 10^8\,{\rm M}_\odot$. The solid (dashed) curve shows $\xi(M, m, z, r)$ obtained using the non-linear (linear) bias approximation, while the histogram shows the two-point correlation function derived from a seminumerical simulation (see text). The non-linear bias formalism matches the simulation better (as shown by Iliev et al. 2003), and therefore provides a more accurate description of clustering of closely separated haloes. Note that in the range of $r \approx$ 10–100 (comoving) kpc, the two-point function in the non-linear case exceeds the linear-bias prediction by one to two orders of magnitude.

The ionizing and LW flux received from a halo of mass m at a distance r depends on the UV emissivity of this particular halo, which is likely to be variable (while this paper was reviewed, Lee et al. 2008 posted a paper that presents a detailed study of the variation of UV luminosity with halo mass), as we discuss next.

2.1.2 The UV luminosity of dark matter haloes

For the UV luminosity of a DM halo, we adopt the empirical relation $L_{\rm LW} \sim 8 \times 10^{27}\,\dot{M}_*$ erg s^{-1} Hz^{-1} (Kennicutt 1998), where $\dot{M}_*$ is the star formation rate inside the halo in units of ${\rm M}_\odot\,{\rm yr}^{-1}$.

The star formation rate in DM haloes is highly uncertain (one of the reasons being radiative feedback itself), especially at the redshifts of interest ($z \sim 10$) where essentially no data exists. The best constraints on the efficiency of star formation in the high-redshift universe are provided by observations of $z \sim 6$ galaxies, which populate a universe that is 'only' 0.5 Gyr older than at $z \sim 10$. Among observed galaxy samples, the $z \sim 6$ population is therefore likely to bear closest resemblance to the $z \sim 10$ population. Note that Stark et al. (2007) have found a few gravitationally lensed emission-line objects, which provide possible candidates for $z = 10$ Lyα emitting galaxies. The small number of candidates, and the small volume that they populate, prohibit strong constraints on the global star formation efficiency at $z = 10$. However, if the candidates are indeed $z = 10$ Lyα emitters, then their abundance would imply that star formation is very efficient at $z = 10$ (see fig. 6 of Mesinger & Furlanetto 2008), which would render our estimates below of the fraction of haloes that 'sees' an anomalously large $J_{\rm LW}$ conservative.

One can reproduce the observed rest-frame UV luminosity function of Lyman-break galaxies at $z \sim 6$ in the *Hubble Deep Fields*

Downloaded from https://academic.oup.com/mnras/article/391/4/1961/1747710 by Scuola Normale Superiore Biblioteca user on 12 December 2025

Table 1. The relation between the parameters $\sigma_{\rm LW}$ and $\mathcal{F}$ that are used to model the scatter in UV luminosity for a given halo mass (see equation 3).

$\sigma_{\rm LW}$	0.0	0.25	0.50	0.66
$\mathcal{F}$	1.0	0.88	0.38	0.21

(Bouwens et al. 2006) by simply assuming that a fraction $\epsilon_{\rm DC} \sim 0.1$ of all DM haloes are converting $f_* \sim 0.1$ of their gas into stars over their duty cycle of $\epsilon_{\rm DC}\, t_{\rm hub} \sim 0.1 t_{\rm hub}$, where $t_{\rm hub}$ is the Hubble time (Wyithe & Loeb 2006). Furthermore, such a model also successfully reproduces the observed luminosity functions of Lyα emitting galaxies at $z = 5.7$ and 6.5 (e.g. Dijkstra, Wyithe & Haiman 2007), which suggests it provides a decent prescription of star formation at $z \sim 6$. If we apply the same star formation efficiency to the haloes of interest, then we find that

$$\langle L_{\rm LW,26}\rangle(m) = 2.8\left(\frac{m}{10^8\,{\rm M}_\odot}\right)\left(\frac{1+z}{11.0}\right)^{-1.5}, \quad (2)$$

where the UV luminosity is in units of 10^{26} erg s^{-1} Hz^{-1}.

Equation (2) implies a one-to-one relation between the mass m of a DM halo and its UV emissivity. However, in the local universe the UV luminosity varies by orders of magnitude for a given stellar mass (e.g. fig. 7 of Schiminovich et al. 2007).

In this paper, we model the spread in UV luminosity produced in haloes with haloes of mass m with a lognormal distribution, $P(L_{\rm LW,26}, m)$. The quantity $L_{\rm LW,26}$ here denotes the LW luminosity per unit star formation rate, in units of 10^{26} erg s^{-1} Hz^{-1}. The probability that a halo of mass m has a UV luminosity in the range $\log L_{\rm x} \pm d\log L_{\rm x}/2$ ('x' denotes 'LW,26') is given by

$$P(\log L_{\rm x}, m)\,{\rm d}\log L_{\rm x} = \frac{{\rm d}\log L_{\rm x}}{\sigma_{\rm x}\sqrt{2\pi}}\exp\left[\frac{-(\log L_{\rm x} - \log[\mathcal{F}\langle L_{\rm x}\rangle])^2}{2\sigma_{\rm x}^2}\right], \quad (3)$$

where log denotes $\log_{10}$. In this paper, our fiducial model adopts $\sigma_{\rm LW} = 0.50$. Hence, the LW flux is larger/smaller by an order of magnitude than the value given by equation (2) for 2.5 per cent of the haloes (for all m). The factor $\mathcal{F}$ reduces the mean luminosity $\langle L_{\rm x}\rangle$ relative to the no-scatter prediction in equation (2). Since the inclusion of scatter increases the predicted abundance at fixed UV luminosity, this factor is necessary to maintain consistency between our model and the observed $z = 6$ rest-frame UV luminosity function (Bouwens et al. 2006). In our fiducial model, we find $\mathcal{F} = 0.38$; increasing $\sigma_{\rm LW}$ requires lower values of $\mathcal{F}$ (see Table 1). We emphasize that the distribution given by equation (3) is clearly ad hoc – it is meant to crudely represent the luminosity scatter one may reasonably expect among high-redshift haloes. The impact of varying the parameter $\sigma_{\rm LW}$ is discussed in Section 3.3.

2.2 Monte Carlo realizations of the model

The environment of a halo is sampled by N_r concentric spherical shells from $r = r_{\rm min}$ out to a maximum radius $r_{\rm max}$. We denote the radius and thickness of shell number j by r_j and ${\rm d}r_j$, respectively. Furthermore, the mass function ${\rm d}n_{\rm ST}(m, z)/{\rm d}m$ is sampled by N_m mass bins that are spaced evenly in $\log m$. Mass bin number i contains haloes in the mass range $\log m_i \pm d\log m_i/2$.

2.2.1 The clustering of sources around a halo

Equation (1) gives the average number of haloes $\mathcal{N}(m, r)\,{\rm d}m\,{\rm d}r$ within the mass range $m \pm {\rm d}m/2$ and within the spherical shell at $r \pm {\rm d}r/2$. The actual number $N(m_i, r_j)$ in shell number j in the ith mass bin fluctuates around this average, and in the MC simulation we populate this shell with haloes by drawing from a Poisson distribution with a mean $\langle N\rangle_{\rm i,j} \equiv \mathcal{N}(m_i, r_j)\,{\rm d}m_i\,{\rm d}r_j$.

2.2.2 The UV luminosity of the surrounding haloes

As mentioned above, only a fraction $\epsilon_{\rm DC} \sim 0.1$ of all haloes are actively forming stars at a given time. We determine whether a halo is 'on' or 'off' by generating a random number $0 \le R \le 1$. If $R \le \epsilon_{\rm DC}$, then the halo is 'on' (i.e. star forming) and vice versa. For each star-forming halo that occupies radial shell number j and mass bin number i, we generate UV luminosities $L_{\rm x}(m_i)$ from the probability distribution given in equation (3) above. Specifically, we convert uniformly distributed random numbers $0 \le R \le 1$ to luminosities $\log L_{\rm x}(m_i)$ using

$$R = \int_{-\infty}^{\log L_{\rm x}(m_i)} P(u, m_i)\,{\rm d}u. \quad (4)$$

This equation can be inverted analytically and yields $\log L_{\rm x}(m_i) = \log[\mathcal{F}\langle L_{\rm x}\rangle(m_i)] + \sigma_{\rm x}\sqrt{2}{\rm erf}^{-1}(2R-1)$, where ${\rm erf}^{-1}$ is the inverse error function, and $\langle L_{\rm x}\rangle(m)$ is given by equation (2).

2.3 The UV flux at the halo

Using the prescription of Section 2.2 for populating the environment of a (single) halo with UV emitting galaxies, we can calculate the LW flux that is 'seen' by the halo from

$$J_{\rm LW} = \frac{1}{4\pi}\sum_{i=1}^{N_{\rm m}}\sum_{j=1}^{N_{\rm r}}\sum_{k=1}^{N(m_i,r_j)}\frac{L_{\rm LW,k}(m_i)}{4\pi r_j^2}\Delta(R - \epsilon_{\rm DC,k}). \quad (5)$$

Here $\Delta(x)$ is the Heavyside step function, and the factor $1/4\pi$ preceding the summation symbols converts the units of $J_{\rm LW}$ into erg s^{-1} cm^{-2} Hz^{-1} sr^{-1} (the units of $L_{\rm LW}$ are erg s^{-1} Hz^{-1}). The sum over k reflects the fact that any given mass-radius bin may contain >1 haloes. For sufficiently large radii and low masses, we often have $\langle N\rangle_{\rm i,j} \gg 1$. In this case, we do not generate UV luminosities for individual haloes. Instead, whenever $\langle N\rangle_{\rm i,j} \ge 10$, the total UV luminosity from that shell is given by its mean value, i.e. $L_{\rm x,i,j} = \langle N\rangle_{\rm i,j}\epsilon_{\rm DC}\langle L_{\rm x}\rangle(m_i)$. This approximation speeds up the calculation, and does not affect the $J_{\rm LW}$ PDF in the tail. The main reason is simple: the high-$J_{\rm LW}$ tail of the PDF arises from Poisson fluctuations in the number of haloes in the inner radial shells, and from fluctuations in the UV luminosity of these sources (see below).

Equation (5) gives the LW flux that is seen by a single halo. We repeat the MC calculation $N_{\rm mc}$ times in order to derive an accurate PDF of $J_{\rm LW}$. We would like to investigate whether haloes exist that are irradiated by an LW background that exceeds $J_{\rm crit} = 10^3$, so that the gas inside these haloes may collapse directly into a massive BH. This scenario was introduced as a possible formation mechanism for the seeds of $z = 6$ SMBHs (see Section 1). These BHs are extremely rare, with a number density of $\sim$1 (comoving) Gpc^{-3} (e.g. Fan et al. 2001, 2003). Hence (approximately) only one halo per cGpc^3 needs to yield a seed. For comparison, there are $\sim 10^9$ haloes at $z = 10$ with virial temperatures exceeding $T_{\rm vir} = 10^4$ K in a 1 cGpc^3 volume. Ideally, we would therefore want to perform $N_{\rm MC} \sim 10^9$ MC simulations, and verify whether at least one halo is exposed to an LW flux that exceeds $J_{\rm crit}$. However, this is computationally prohibitively expensive. In practice, we instead utilize $N_{\rm MC} \sim 10^7$ realizations, and complement our MC simulations with analytic calculations as described in Section 3.3.

Downloaded from https://academic.oup.com/mnras/article/391/4/1961/1747710 by Scuola Normale Superiore Biblioteca user on 12 December 2025

Table 2. Fiducial model parameters (see Section 3.1 for discussion).

M ($M_\odot$)	$m_{\rm min}$ ($M_\odot$)	$r_{\rm min}$ (pkpc)	$r_{\rm max}$ (pMpc)	$\sigma_{\rm LW}$	$N_{\rm mc}$
4×10^7	4×10^7	$2r_{\rm vir} = 2.0$	18	0.50	10^7

3 RESULTS

We use $N_m = 500$ and $N_r = 100$ throughout this paper. We have verified that our results are not sensitive to the precise choices of N_m and N_r.

3.1 The model parameters

In our fiducial model, we investigate the flux PDF seen by haloes of mass $M = M_{\rm H} = 4 \times 10^7$ $M_\odot$ at $z = 10$. These haloes are just massive enough to excite atomic H cooling processes (i.e. $T_{\rm vir} = 10^4$ K, e.g. equation 25 in Barkana & Loeb 2001, for a mean molecular weight $\mu = 1.2$). As mentioned above, the number density of sources more massive than $M_{\rm H}$ at $z = 10$ is $\sim$1 cMpc^{-3}. The impact of varying M is investigated in Section 3.3.

The minimum distance of the centre of the halo to the centre of another nearby halo, $r_{\rm min}$, has to be specified in our model. In the absence of peculiar velocities, one may expect $r_{\rm min} > r_{\rm vir,M}$. However, close pairs of haloes can merge, and share a common halo, making $r_{\rm min} < r_{\rm vir,M}$ possible. On the other hand, (very) close halo pairs are short-lived, and will merge on a time-scale shorter than $\epsilon_{\rm DC} t_{\rm hub}$. The precise choice of $r_{\rm min}$ is therefore somewhat arbitrary; in the fiducial model we adopt $r_{\rm min} = 2r_{\rm vir} = 2.0$ kpc, and we will investigate the impact of varying $r_{\rm min}$ in Section 3.3.

In our calculation, we only consider haloes out to $r_{\rm max} = (\lambda_{\rm LW,1} - \lambda_\beta)c/[\lambda_\beta H(z)] \sim 18$ pMpc, in which $\lambda_{\rm LW,1} = 1110$ Å is the wavelength corresponding to the lowest energy LW transition. LW photons that were emitted at $r > r_{\rm max}$ have redshifted into one of the Lyman series resonances prior to reaching the halo, and are converted efficiently into photons with energies $<$10.2 eV before reaching our halo. In reality, 18 pMpc is an upper limit, and $r_{\rm max}$ should be a strong function of frequency (Haiman et al. 1997). The impact of LW radiative transfer on our results is discussed further in Section 4.1; in practice, the high-flux tail of the PDF is insensitive to the choice of $r_{\rm max}$.

Finally, we assume that the minimum mass for star-forming haloes is $m_{\rm min} = 4 \times 10^7$ $M_\odot$. This model therefore represents a universe in which no star formation occurs in 'minihaloes' with $T_{\rm vir} = 10^4$ K (e.g. due to the presence of the LW background itself or due to an X-ray background). The impact of varying $m_{\rm min}$ is investigated in Section 3.3. The parameters of our fiducial model are summarized in Table 2.

3.2 The flux PDF in the fiducial model

In Fig. 2, we show our main results: histograms showing the fraction of MC realizations that yield an LW flux $J_{\rm LW}$ as a function of $J_{\rm LW}$. The solid histogram shows the fiducial model. The distribution in $J_{\rm LW}$ peaks at around $J_{21,\rm LW} = 40$, and 95 per cent of the models lie in the range $35 \lesssim J_{21,\rm LW} \lesssim 45$. The distribution is highly asymmetric with a long tail towards high values of $J_{21,\rm LW}$.

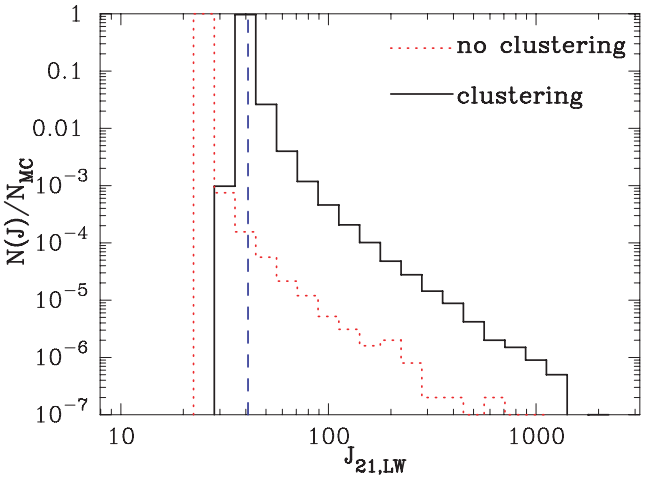

Figure 2. The probability distribution (PDF) of the LW flux $J_{\rm LW}$ (in units of $J_{21,\rm LW} = 10^{-21}$ erg s^{-1} cm^{-2} sr^{-1} Hz^{-1}) as seen by haloes of mass $M = 4 \times 10^7$ $M_\odot$ at $z = 10$. The black solid (red dotted) histogram corresponds to our fiducial model with (without) clustering. The dashed vertical line at $J_{21,\rm LW} = 40$ denotes the mean value of the LW background (see text). The figure shows that (i) the vast majority of haloes see an LW flux that is within a factor of 2 of the mean value, (ii) the clustering of haloes boosts the tail of the flux PDF by more than an order of magnitude and (iii) an exceedingly small, but non-zero fraction ($\sim$ few $\times 10^{-7}$) of DM haloes see an LW flux boosted to levels exceeding $J_{21,\rm LW} > J_{\rm crit} = 10^3$.

The sharp cut-off on the low-$J_{21,\rm LW}$ side is due to the fact that the IGM is assumed to be transparent to LW photons, which causes a large number of distant sources to contribute to the intensity of the local LW radiation field (for reference, the total number of haloes with $m > m_{\rm min}$ within a sphere of radius $r_{\rm max} = 18$ pMpc is $\gtrsim 10^7$!). Poisson fluctuations in a large number of distant sources, as well as variations in their UV luminosity, only result in a small variation in $J_{\rm LW}$. Indeed, the dashed vertical line at $J_{21,\rm LW} = 40$ corresponds to the value of $J_{\rm LW}$ in the absence of any scatter in UV luminosity of individual haloes (i.e. $\sigma_{\rm LW} = 0.0$), and with no Poisson fluctuations in the number of haloes. This can be thought of as the level of the global mean LW background. No haloes see a flux that is significantly smaller than this mean background value of $J_{21,\rm LW} = 40$ (i.e. among our 10^7 realizations, and with our flux bin resolution, there are no instances when the flux falls below the lowest flux bin). Note that this value differs for the runs that do and do not include clustering.

On the other hand, the long tail towards high $J_{21,\rm LW}$ arises from Poisson fluctuations in the number of close haloes, and from the assumed scatter in their UV luminosity. The highest values of $J_{21,\rm LW}$ are seen by haloes that have a luminous nearby neighbour. This is illustrated graphically in the left-hand panel of Fig. 3, where we show the environment of a halo that is irradiated by an LW flux close to the maximum value we find, $J_{21,\rm LW} \sim 10^3$. The small (red) square at $x = y = 0$ kpc denotes the position of the central halo, while open circles denote haloes in which no star formation occurs, and are therefore not producing any LW flux. The filled circles denote haloes that are forming stars, with the magnitude of the UV luminosity represented by the size of the circles. For reference, the sizes corresponding to $L_{\rm LW,26} = 1.0, 10.0$ and 100.0 are shown as labelled above the figure panels. The central halo is illuminated by

Downloaded from https://academic.oup.com/mnras/article/391/4/1961/1747710 by Scuola Normale Superiore Biblioteca user on 12 December 2025

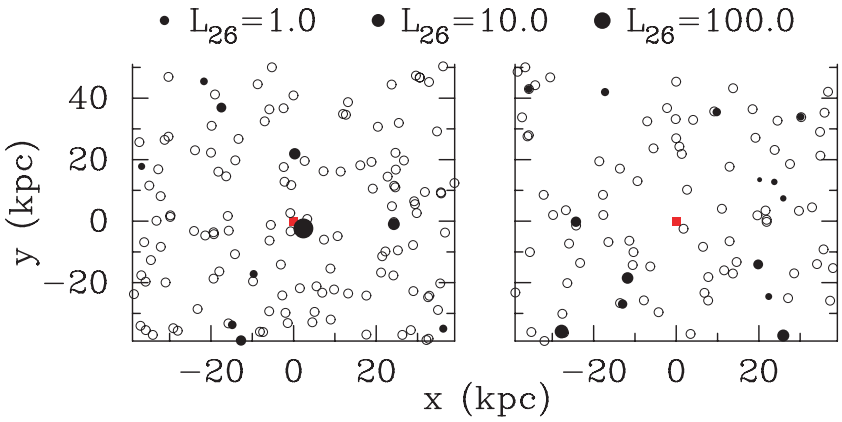

Figure 3. Two realizations of the environment of a fiducial $M = 4 \times 10^7\,M_\odot$ halo at $z = 10$. The left-hand (right-hand) panel shows a halo that 'sees' a $J_{21,LW} = 10^3$ ($J_{21,LW} = 40$). The fiducial halo is represented by the filled square at $x = y = 0$ kpc. Open circles denote surrounding galaxies that are not actively forming stars, and therefore not contributing to the local LW flux. Solid circles denote haloes that are actively forming stars; their UV luminosity is represented by the size of the circle (the largest circles are the most luminous, as illustrated by the graphic scale above the panels). The halo that sees $J_{21,LW} \sim 10^3$ has a nearby ($r \sim 3$ kpc) neighbour that is luminous ($L_{LW,26} = 10^2$), while the halo in the right-hand panel has no luminous nearby neighbour, and sees $J_{21,LW} \sim 40$. The latter configuration is most common.

a bright ($L_{LW,26} \sim 10^2$), nearby ($r \approx 3$ kpc) star-forming halo.[2] For comparison, the right-hand panel shows the environment of a much more common halo that sees $J_{LW,21} = 40$. Here, the nearest source is located at a distance of $r = 25$ kpc and has a UV luminosity of $L_{LW,26} = 10$ (this source only contributes ∼2 per cent of the total LW flux seen by the central halo at $r = 0$).

Note that this figure also illustrates the importance of clustering. Fig. 3 shows the distribution of haloes in a surrounding volume that is ∼0.35 comoving Mpc^3; without clustering, according to the Sheth–Tormen mass function, this volume would contain, on average, only ∼1.4 DM haloes with $T_{vir} \gtrsim 10^4$ K. In the presence of clustering, we find several tens of haloes in both realizations shown in the two panels.

Fig. 2 shows that even though the distribution of J_{LW} drops off rapidly with increasing J_{LW}, the fraction few $\times 10^{-7}$ of all haloes see $J_{21,LW} \geq 10^3$. This corresponds to 10^3 haloes in a volume of 1 Gpc^3. Note that because the high-J_{LW} tail is dominated by close pairs of haloes, accounting for clustering is quite important in the present calculation. This is quantified by the red dotted curve which shows the fiducial model, but without source clustering [i.e. $\xi(M, m, z, r) = 0$ in equation 1]. In the absence of clustering the fraction of haloes that sees a given J_{LW} above the mean value is typically smaller by about 1.5 orders of magnitude.[3]

Our main result, presented in this section, is that a non-negligible fraction of haloes, i.e. a few $\times 10^{-7}$, may see a local LW flux that is higher by almost two orders of magnitude compared to the mean global background (corresponding to a model in which Poisson fluctuations in the number of sources, their clustering and variations in their UV luminosity are ignored). In the next section, we investigate the sensitivity of this result to the assumed model parameters.

3.3 The impact of model-parameter variations

The impact of varying the model parameters on the very high J_{LW} tail of the flux distribution can be efficiently investigated using an analytic approach. This is because the high-J_{LW} tail is dominated by haloes with a nearby star-forming halo, and, in this limit, the Poisson probability of having two or more such nearby haloes is negligibly small. The probability that a halo has *at least one* neighbour that would alone expose it to an LW flux in the range $\log J_{LW} \pm \mathrm{d}\log J_{LW}/2$, is given by

$$P_1(J_{LW})\,\mathrm{d}\log J_{LW} = \mathrm{d}\log J_{LW}\epsilon_{DC} \times \sum_{i=i_{min}}^{N_m}\sum_{j=j_{min}}^{N_r} \langle N\rangle_{i,j}\, e^{-\langle N\rangle_{i,j}}\, P(\log L[J_{LW}, r_j], L_x[m_i]), \quad (6)$$

where $\langle N\rangle_{i,j} = \mathcal{N}(m_i, r_j)\mathrm{d}m_i\mathrm{d}r_j$ (see Section 2.2.1), $r(i_{min}) = r_{min}, m(j_{min}) = m_{min}$ and $P(\log L[J_{LW}, r], L_x[m])\,\mathrm{d}\log J_{LW}$ denotes the probability that a halo of mass m that is located at a distance r produces an LW luminosity in the range $\log J_{LW} \pm \mathrm{d}\log J_{LW}/2$. This halo must have an LW luminosity that is $L = 16\pi^2 r^2 J_{LW}$ (in erg s^{-1} Hz^{-1}), and $P(\log L[J_{LW}, r], L_x[m])\,\mathrm{d}\log J_{LW} = P(\log L, m)\,\mathrm{d}\log L$, for which the expression was given in equation (3).

In Fig. 4, we compare the probability $P_1(J_{LW})\,\mathrm{d}\log J_{LW}$ obtained from equation (6) (dotted curves) with that obtained from the MC simulations (histograms) for the fiducial model (middle panel), and for a model in which σ_{LW} is changed to $\sigma_{LW} = 0.66$ ($\sigma_{LW} = 0.25$) in the top (bottom) panel. Fig. 4 shows that the two methods yield consistent results for $J_{LW,21} \gtrsim 500$ in all three cases. This agreement demonstrates that the high fluxes must be dominated by a single nearby source, and that we can safely use equation (6) to compute the J_{LW} probability distribution for $J_{21,LW} \gtrsim 500$. At lower values of $J_{21,LW}$, the Poisson probability of having more than one nearby UV bright star-forming halo can become non-negligible. To examine this possibility, we define the probability that a halo has *either* at

[2] Our spherically symmetric clustering model generates only radial distances; we have artificially generated random azimuthal angles to place the haloes in the *xy* plane in Fig. 3. Hence, Fig. 3 does not represent an accurate projection or slice of a realistic 3D source distribution; it is meant only to graphically illustrate the difference in the environment of haloes illuminated by a high versus a low J_{LW}.

[3] The enhancement of the high-flux tail of the PDF due to clustering varies only weakly with $J_{21,LW}$. The reason for this weak dependence is that especially the tail end of the PDF at $J_{LW,21} \gtrsim 200$ arises mainly from single UV sources that are in close proximity ($2 < r < 7$ kpc, see Section 3.3) to the central halo. Over this narrow range of separations, the two-point function $\xi(M, m, z, r)$ – and hence the expected number of surrounding haloes – varies relatively weakly (the clustering length for haloes of mass M is ∼300 pkpc, see Fig. 1).

Downloaded from https://academic.oup.com/mnras/article/391/4/1961/1747710 by Scuola Normale Superiore Biblioteca user on 12 December 2025

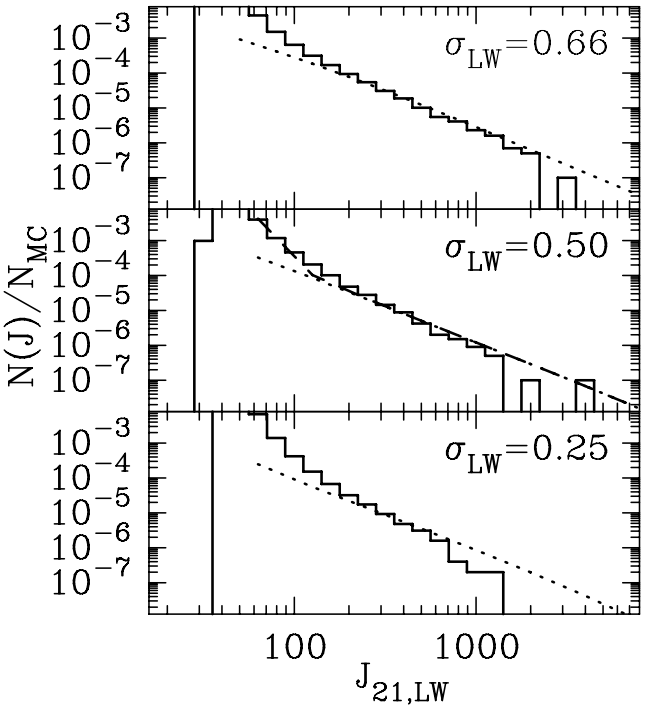

Figure 4. The probability $P_1(J_{\rm LW})$ for a halo to have a neighbour that would alone expose it to an LW flux of $J_{\rm LW}$ is shown by the dotted curves (obtained from equation 6), and compared to the flux PDF obtained from MC simulations (histograms). The fiducial model is shown in the middle panel, while in the top panel (bottom panel) the luminosity scatter $\sigma_{\rm LW}$ is increased (decreased) to $\sigma_{\rm LW} = 0.66$ ($\sigma_{\rm LW} = 0.25$). Both methods yield consistent results for $J_{\rm LW,21} \gtrsim 500$ for all models, demonstrating that the high-$J_{21,\rm LW}$ tail of the $J_{\rm LW}$ distribution is dominated by a single nearby star-forming halo, and that the analytic approach can be used to extrapolate the probability distribution of $J_{\rm LW}$ beyond $J_{21,\rm LW} \gtrsim 500$. The dashed curve in the middle panel shows a variation of the analytical prediction that accounts for *pairs* of neighbouring haloes producing the combined flux $J_{\rm LW}$. The agreement at lower values of $J_{21,\rm LW}$ is better, indicating that at $J_{\rm LW,21} \lesssim 500$, often two haloes contribute significantly to the total flux.

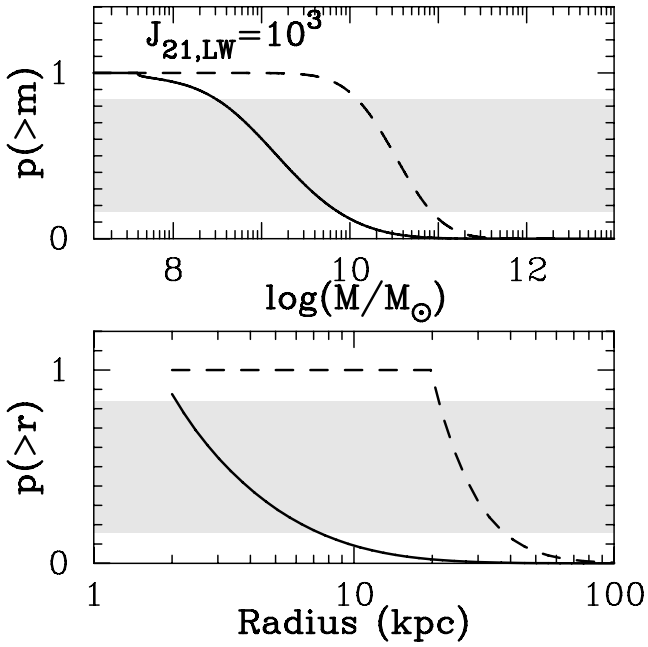

Figure 5. The cumulative probabilities for the mass (top panel) and location (bottom panel) of the single halo that produces $J_{21,\rm LW} = 10^3$ in the fiducial model (solid curves) and for a model in which $r_{\rm min} = 20$ kpc (dashed curves). The light grey regions denote the central 68 per cent, or 1σ, confidence interval. The figure shows that in the fiducial model, the most probable cases are low-mass haloes (in the range $3 \times 10^8 < m < 6 \times 10^9\,{\rm M}_\odot$) located very nearby ($2 < r/{\rm kpc} < 7$). The halo mass and distance are both boosted for the model in which $r_{\rm min}$ is increased to 20 kpc.

least one neighbour that would alone expose it to an LW flux in the range $\log J_{\rm LW} \pm {\rm d}\log J_{\rm LW}/2$ (as before), *or* it has at least *one pair* of neighbours whose combined flux equals $\log J_{\rm LW} \pm {\rm d}\log J_{\rm LW}/2$. In the latter case, the two haloes are required to produce intensities of $yJ_{\rm LW}$ and $[1-y]J_{\rm LW}$, respectively, with $0 < y < 1$. For a given fractional allocation y of the flux between the two haloes, $P_2(J_{\rm LW})\,{\rm d}\log J_{\rm LW}$ is given by $P_2(y) \propto \{P_1(yJ_{\rm LW})\,P_1([1-y]J_{\rm LW})\}$, and the total probability for at least one such pair of neighbours is given by $P_{2,\rm tot} = \int_0^1 {\rm d}y\,P_2(y)$. As an example, the dashed curve in the middle panel of Fig. 4 shows the probability $P_1 + P_{2,\rm tot}$ as a function of $J_{\rm LW}$. Clearly, accounting for pairs of haloes provides a better fit to the MC simulations at lower values of $J_{21,\rm LW}$.

In Fig. 5, we investigate the most likely host halo mass and distance of the nearby UV source producing the critical flux. In the top panel, we plot the cumulative probabilities for the mass of the halo that produces $J_{21,\rm LW} = 10^3$ in the fiducial model (solid curve), and for a model in which $r_{\rm min} = 20$ kpc (dashed curve). This cumulative probability is given by replacing $m_{\rm min} \rightarrow {\rm m}$ as the lower limit in the mass integral in equation (6). The solid curve shows that in the fiducial model, the halo mass lies in the range $3 \times 10^8 < m < 6 \times 10^9\,{\rm M}_\odot$, while its most likely position is $2 < r/{\rm kpc} < 7$ [the shaded ranges enclose 68 per cent of the total probability around $p(>x) = 0.50$]. The most likely halo mass is increased to lie in the range $\approx 10^{10} < m < 8 \times 10^{10}\,{\rm M}_\odot$ for the model in which $r_{\rm min} = 20$ kpc.

In the bottom panel, we plot the cumulative distribution that the star-forming halo was located at a distance that exceeds r (given by replacing $r_{\rm min} \rightarrow {\rm r}$ as the lower limit in the radial integral in equation 6). In the fiducial model, the distance to the dominant star-forming halo lies between $2 < r/{\rm kpc} < 7$, while this range is increased to $20 < r/{\rm kpc} < 40<$ for the model in which $r_{\rm min} = 20$ kpc (68 per cent ranges are shaded, as above).

It is interesting to point out that in the fiducial model, the parameter combination $r = 3$ kpc and $m = 10^9\,{\rm M}_\odot$ [for which $p(>r) = p(>m) = 0.5$], results in $J_{21,\rm LW} \sim 200$. Hence, in order for such a halo to produce a local flux of $J_{21,\rm LW} \sim 10^3$, it must be $\sim$5 times brighter than average. Since this corresponds to $\sim 1.4\sigma_{\rm LW}$, this implies we are not very sensitive to the tail end of the assumed lognormal distribution of the UV luminosity of star-forming haloes (indeed, in Fig. 6 we explicitly show that the tail of the flux PDF is not sensitive to $\sigma_{\rm LW}$).

In Fig. 6, we explore the impact of varying the model parameters, M (top panel), $\sigma_{\rm LW}$ (second panel from the top), as shown above in Fig. 4), $r_{\rm min}$ (third panel) and $m_{\rm min}$ (fourth panel). The parameter dependencies seen in this figure are easily understood.

Fig. 6 shows that: (i) the tail end of the flux PDF is boosted slightly for $M = 8 \times 10^7\,{\rm M}_\odot$ (dotted curve) and significantly for $M = 10^9\,{\rm M}_\odot$ (dashed curve), which reflects the fact that sources are clustered more strongly around more massive haloes; (ii) increasing $\sigma_{\rm LW}$ enhances the tail of the flux PDF, but only slightly. The enhancement arises because increasing $\sigma_{\rm LW}$ enhances the probability of having a nearby halo that is (significantly) brighter than

Downloaded from https://academic.oup.com/mnras/article/391/4/1961/1747710 by Scuola Normale Superiore Biblioteca user on 12 December 2025

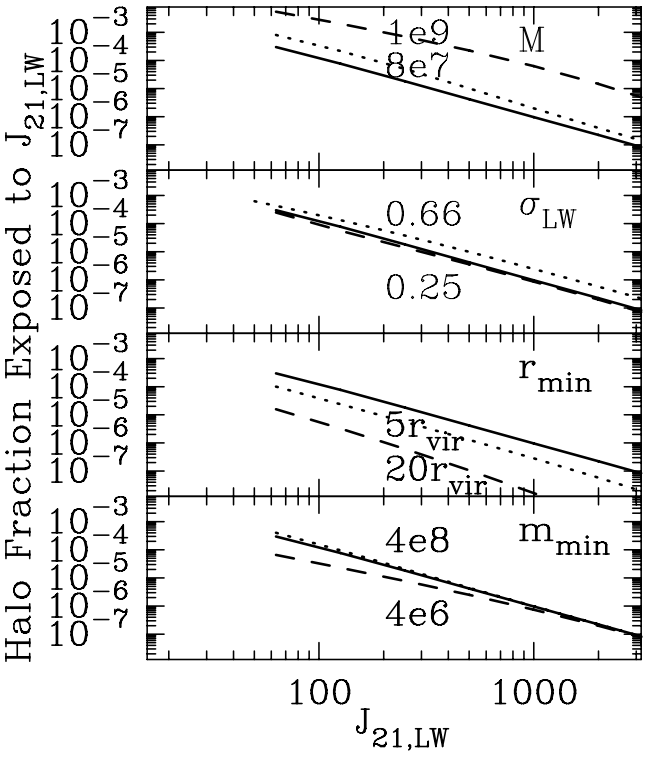

Figure 6. The impact of varying the model parameters, M (top panel), $\sigma_{\rm LW}$ (second panel from the top), $r_{\rm min}$ (third panel) and $m_{\rm min}$ (fourth panel) on the $J_{\rm LW}$ probability distribution is shown. This figure demonstrates that our results are most sensitive to the precise values of M and $r_{\rm min}$. Increasing M ($r_{\rm min}$) significantly boosts (reduces) the high-flux tail. However, even an increase of $r_{\rm min}$ by a factor of 10 results in a non-negligible fraction of haloes that are exposed to a $J_{21,\rm LW} = J_{\rm crit} = 10^3$ (see text).

average in the UV[4]; (iii) increasing $r_{\rm min}$ decreases the tail at high $J_{\rm LW}$. This is because increasing $r_{\rm min}$ eliminates the contribution of very nearby haloes to the $J_{\rm LW}$ distribution (this conclusion can already be inferred from Fig. 5, which shows that the most nearby haloes dominate the single-halo flux); (iv) increasing $m_{\rm min}$ reduces the flux PDF at $J_{21,\rm LW} \lesssim 500$, but the high-flux tail is not significantly affected. This is because the highest values of $J_{21,\rm LW}$ require LW luminosities that are $L = 6 \times 10^{27}\,(r_{\rm min}/2\,{\rm kpc})^2 (J_{21,\rm LW}/10^3)$ erg s^{-1} Hz^{-1}. Hence, producing these fluxes requires the presence of a source that is forming stars at a minimum rate of $\sim 0.7\,{\rm M}_\odot\ {\rm yr}^{-1}$. Prolonged star formation rates of this magnitude can only occur in haloes that are more massive than $2 \times 10^8\,{\rm M}_\odot$. Therefore, any variation of $m_{\rm min}$ has a negligible impact on the flux PDF at $J_{21,\rm LW} \gtrsim 500$, as long as $m_{\rm min} \lesssim 2 \times 10^8\,{\rm M}_\odot$ (which seems likely prior to the completion of reionization, e.g. Mesinger & Dijkstra (2008).

[4] Consider a halo of mass $m = 4 \times 10^7\,{\rm M}_\odot$ that is located at $r = 2$ kpc. In the fiducial model, this source needs to be $\gtrsim$60 times brighter than average to produce $J_{\rm LW,21} \gtrsim 10^3$, which corresponds to $\gtrsim 3.6\,\sigma$. On the other hand, this same source needs to be $\sim$100 times brighter than average in the model in which $\sigma_{\rm LW} = 0.66$ (because the factor $\mathcal{F}$ scales the mean UV luminosity to remain consistent with the observed $z = 6$ luminosity function of LBGs, see Table 1), which in this model corresponds to $\gtrsim 3.1\sigma$. Boosting $\sigma_{\rm LW}$ therefore boosts the number of sources capable of producing $J_{\rm LW,21} \gtrsim 10^3$ (but only slightly).

4 DISCUSSION

4.1 Lyman–Werner radiative transfer

The dissociation of H_2 molecules follows photoexcitation of their electronic states. There are 76 of these LW transitions, the majority of them having energies that lie blueward of the Lyβ resonance (see e.g. fig. 1 of Haiman et al. 2000). The majority of photons that are capable of dissociating H_2 molecules have therefore redshifted into the Lyβ resonance over a distance that is much smaller than the $r_{\rm max}$ that was used in our model. In fact, $r_{\rm max}$ should have a strong frequency dependence (e.g. some of the LW lines are just on the red side of an atomic H Lyman line; photons could not have suffered significant redshift before reaching such frequencies without scattering, implying small $r_{\rm max}$ at the frequency of these LW lines).

The overall conclusion is that the total photodissociation rate due to far away sources is reduced, and that our simple modelling which ignores radiate transfer in the IGM overestimates the value of the global mean LW background. Additionally, a trace fraction of molecular hydrogen in the IGM ($x_{\rm H_2} \sim 2 \times 10^{-6}$) is sufficient to produce an effective optical depth in the LW lines of $\tau_{\rm H_2} \sim 1$–2 (Ricotti, Gnedin & Shull 2001). Furthermore, $x_{\rm H_2}$ may be enhanced inside 'relic H_2 regions', which increases the volume-averaged effective optical depth of the IGM in the LW lines (Johnson, Greif & Bromm 2007, also see Shapiro & Kang 1987. Kuhlen & Madau (2005) have shown recently that X-rays produced by the first generation of accreting BHs may boost the fraction of intergalactic H_2 by a factor of $\sim$20 around such 'miniquasars'. If the IGM is optically thick in the LW lines, then $r_{\rm max}$ becomes an even stronger function of frequency.

We next investigate the assumption that the IGM is optically thick in every one of the H_2 lines. Note that this is a very conservative assumption, requiring that the photodissociated intergalactic H_2 is continuously replenished, which is unlikely to be the case (Haiman et al. 2000); we purse this assumption here because it maximizes the impact of RT effects.

In Fig. 7 the red dotted histogram shows the LW flux PDF that is obtained when taking into account this strong frequency dependence of $r_{\rm max}$. We modelled this frequency dependence by computing the maximum distance $r_{\rm max}(k)$ from which LW[k] photons (the kth LW transition, when the 76 LW lines are ranked simply in order of increasing energy) can be received, i.e. $Hr_{\rm max}(k)/c = (\lambda_k - \lambda_{k+1})/\lambda_{k+1}$. Here, λ_k denotes the wavelength of the kth LW transition. LW[k] photons cannot by received from sources at larger radii, as these photons redshifted through the LW[$k+1$] resonance first, which makes the IGM effectively optically thick to sources beyond $r_{\rm max}(k)$. A source at radius r then contributes the following flux to the local LW background:

$$J_{\rm LW} = \frac{1}{4\pi}\frac{L_{\rm UV}}{4\pi r^2}\frac{k_{\rm diss}}{k_{\rm tot}},$$

where $k_{\rm tot}$ is the total photodissociation rate as summed over all 76 transitions, and where $k_{\rm diss}$ is the photodissociation rate that one obtains if one sums over only over those lines for which $r < r_{\rm max}(k)$.

Fig. 7 shows that in the above, conservative, optically thick limit, our neglect of LW radiative transfer overestimates the value of the mean LW background by about an order of magnitude, and underestimates the width of the flux PDF. However, the high-$J_{\rm LW}$ tail of the flux PDF depends entirely on the statistics and nature of very nearby star-forming haloes (within a few to a few tens of kpc).

Downloaded from https://academic.oup.com/mnras/article/391/4/1961/1747710 by Scuola Normale Superiore Biblioteca user on 12 December 2025

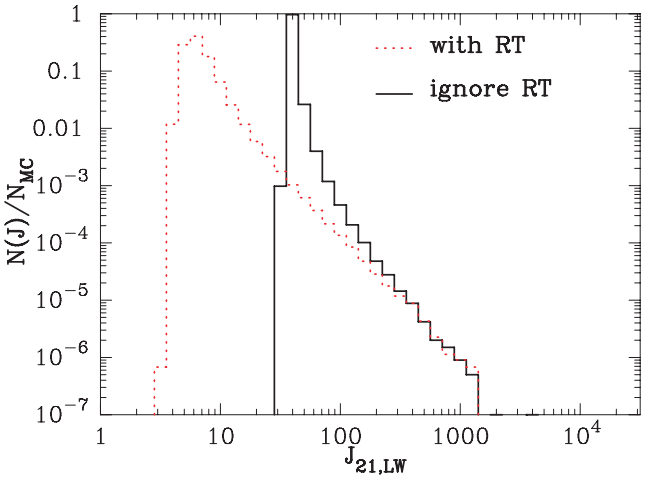

Figure 7. We show the LW flux PDF for the fiducial model (solid black histogram, as in Fig. 2), and for a model in which intergalactic H_2 reduces the photodissociation rate due to far away sources, which in turn reduces the value of the global mean LW background by about an order of magnitude. However, the high-$J_{\rm LW}$ tail of the flux PDF depends entirely on the statistics and nature of very nearby star-forming haloes, and LW radiative transfer effects from the IGM do not affect this tail of the $J_{\rm LW}$ probability distribution at all.

LW radiative transfer effects from the IGM do not affect this tail of the $J_{\rm LW}$ probability distribution at all, even in this extreme limit.

We also note that LW photons dominate the H_2 dissociation rate when the medium is optically thick and lacks radiation above 13.6 eV. Indeed, the critical value of $J_{\rm crit} \sim 10^3$ corresponds to the photodissociation time *due to LW radiation* being shorter than the free-fall time of the gas. In our case, the column density of neutral H I out to the nearby star-forming neighbour is likely negligible, and direct photodissociation by photons with energies $E > 15.4$ eV will boost the total H_2 dissociation rate (the latter dominates for neutral H I column densities $N_{\rm H\,I} \lesssim 10^{19}$ cm^{-2}; Haiman et al. 1997). This may help to keep the halo gas H_2-free, at least during the early stages of its collapse (until contraction results in a column density exceeding $N_{\rm H\,I} \sim 10^{19}$ cm^{-2}).

Lastly, it is worth pointing out that since the tail of the flux PDF is due to a single neighbour, the impinging LW radiation field is highly anisotropic. The impact of an anisotropic radiation field on the gas could be quite different from that of an isotropic background (e.g. perhaps the 'far side' can be shielded more efficiently against the impinging photodissociating flux, which could allow gas to cool and fragment), but a quantitative assessment of this 3D behaviour is beyond the scope of this paper.

4.2 The evolutionary phase of the halo/timing issues

We have found that a fraction of a few $\times 10^{-7}$ of all $z = 10$ DM haloes with $T_{\rm vir} \geq 10^4$ K are irradiated by an LW flux that exceeds $J_{\rm crit}$ (Fig. 6). However, the direct-collapse BH scenario requires that the gas is irradiated and kept H_2-free for the entire $\sim$ free-fall time while it collapses to the centre of the DM halo. This additional requirement reduces the fraction of DM haloes in which these BHs may form.

To quantify this reduction, we identify three relevant time-scales: (i) the duration over which haloes are producing UV luminosity ($t_{\rm lum}$). In our model, this corresponds to $t_{\rm lum} = \epsilon_{\rm DC} t_{\rm hub}$; (ii) the duration over which the irradiation is needed to avoid fragmentation ($t_{\rm frag}$) and (iii) the spread in formation times of neighbouring haloes ($t_{\rm form}$). In our model, we implicitly assumed that $t_{\rm form} = t_{\rm hub}$ (since we only assumed that a fraction $\epsilon_{\rm DC}$ of all haloes are actively forming stars). The overall likelihood for a combination of two haloes in which one prohibits fragmentation in the other is given by the fraction of occasions in which one halo formed within a time $t_{\rm lum} - t_{\rm frag}$ prior to the other during a time $t_{\rm form}$. If the formation times of both haloes are uncorrelated, then this probability is given by $q = (t_{\rm lum} - t_{\rm frag})/t_{\rm form}$. If we write $t_{\rm frag} \equiv t_{\rm lum}/f$, then we find that $q = (1 - 1/f)$. In this case, the reduction due to the synchronization requirement is small for $f \gtrsim 2$. Furthermore, the reduction is significantly less, if the formation times of the two haloes are correlated (which is very likely, since both the collapsing and the star-forming halo formed in the same large-scale overdense region of the universe).

4.3 The importance of photoheating

The haloes of interest that are irradiated by a large LW flux are also illuminated by ionizing radiation, with an ionizing flux that is lower by a factor of $f_{\rm esc}$ (the escape fraction of ionizing photons) than $J_{\rm LW}$. This escape fraction is highly uncertain: recently, Chen, Prochaska & Gnedin (2007) have derived a distribution function for $f_{\rm esc}$ from the cumulative H I column density distribution along sightlines to (long-duration) γ-ray burst (GRB) afterglows. Long-duration GRBs are thought to be associated with massive ($M \gtrsim$ 10–30 $M_\odot$) young stars, and are therefore thought to occur within star-forming regions of galaxies (see e.g. Woosley & Bloom 2006). GRB afterglows may therefore probe the H I column density along sightlines to the production sites of ionizing photons.[5] Chen et al. (2007) show that $f_{\rm esc}$ may obtain a wide range of values, and that $\langle f_{\rm esc} \rangle = 0.02$, in good agreement with theoretical calculations of the escape fraction of ionizing photons from galaxies in adaptive mesh refinement hydrodynamical simulations[6] by Gnedin, Kravtsov & Chen (2008).

From the above we conclude that the haloes of interest may be irradiated by a ionizing flux that likely has a broad distribution between $J_{\rm ion,21} = 0$–10^3, with $\langle J_{\rm ion,21} \rangle \sim 20$. To investigate the impact of this photoionizing flux on the dynamics of the gas in collapsing halo, we performed a 1D hydrodynamical simulation with a code that was originally written by Thoul & Weinberg (1995) and modified as described in Dijkstra et al. (2004, where it was used to study the impact of photoionization feedback on the formation of dwarf galaxies). We illuminated a gas cloud of mass $M = 10^8$ $M_\odot$ with an ionizing flux having amplitudes of $J_{\rm ion,21} = 10$ and 10^2, and spectral index $\alpha = 1$ [i.e. the ionizing flux density is given by $J(\nu) = J_{21,\rm ion}(\nu/\nu_{\rm L})^{-\alpha} \times 10^{-21}$ erg s^{-1} Hz^{-1} cm^{-2} sr^{-1}]. This ionizing flux was switched on at a time $\Delta t = \epsilon_{\rm DC}\, t_{\rm hub}$ before the cloud would have collapsed to $r = 0$ in the absence of pressure.

The result of these calculations is shown in Fig. 8. Solid curves show the time evolution of the radii of gas shells enclosing 30, 40, 50 and 100 per cent of the total halo mass in the absence of an

[5] Furthermore, evidence exists that the majority of GRBs occur in sub-L_* galaxies (see Chen et al. 2007, and references therein), which are likely to bear a closer resemblance to the $z = 10$ star-forming galaxies in our model, than the massive LBGs for which escape fractions of ionizing photons have also been determined on the basis of their observed Lyman break (Shapley et al. 2006).

[6] Whalen, Abel & Norman (2004) found $f_{\rm esc} \sim 1$ for galaxies at $z \sim 20$, using 1D hydrodynamic calculation. However, their calculations focused on the first UV sources in the Universe which populated much less massive 'minihaloes'.

© 2008 The Authors. Journal compilation © 2008 RAS, MNRAS **391,** 1961–1972

Downloaded from https://academic.oup.com/mnras/article/391/4/1961/1747710 by Scuola Normale Superiore Biblioteca user on 12 December 2025

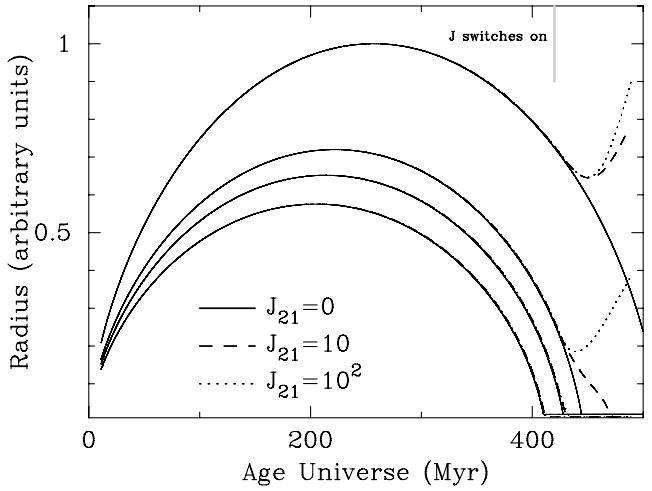

Figure 8. Solid curves show the time evolution of the radii of gas shells during the collapse of 10^8 $M_\odot$ halo, in the absence of an externally generated ionizing radiation field (i.e. $J_{\rm ion,21} = 0$). Each set of curves corresponds to shells (initially) enclosing 30, 40, 50 and 100 per cent of the total halo mass. All gas in the halo has collapsed by $z = 10$, when $t_{\rm hub} \sim 500$ Myr. The dashed (dotted curves) represent models in which an ionizing background, whose amplitude was $J_{\rm ion,21} = 10$ ($J_{\rm ion,21} = 10^2$), was switched at a time $\Delta t = \epsilon_{\rm DC} t_{\rm hub}$ before the cloud would have collapsed to $r = 0$ in the absence of pressure. The figure shows that even when $J_{\rm ion,21} = 10$ ($J_{\rm ion,21} = 10^2$), still 50 per cent (40 per cent) of the gas was able to collapse.

externally generated ionizing radiation field. The dashed (dotted curves) represent the models in which $J_{\rm ion,21} = 10$ ($J_{\rm ion,21} = 10^2$). The figure shows that even when $J_{\rm ion,21} = 10$ ($J_{\rm ion,21} = 10^2$), still 50 per cent (40 per cent) of the gas was able to collapse, which implies that photoionization feedback does not prevent the gas from collapsing, even with extremely high UV fluxes. The main reason for this is that photoionization feedback is most efficient when it can operate for a prolonged time: e.g. in our spherical collapse model, this feedback mechanism has the largest effect when the radiation field is switched 'on' when (or before) the gas completely decouples from the Hubble flow and starts to collapse. However, in the final $\epsilon_{\rm DC} t_{\rm hub}$ of the cloud's collapse, the gas in the halo has already collapsed to densities that greatly exceed the mean cosmic gas density in the Universe, and cooling processes are more efficient. Furthermore, at these high gas densities self-shielding, which is ignored in our simulation, will become important which would make photoionization feedback even less important.

Lastly, it is worth pointing out that haloes form, and cluster strongly, at intersections of filaments. The dominating LW flux will therefore be emitted by haloes along the filaments. On the other hand, their ionizing flux will most likely escape into the low-density regions, perpendicular to the filaments. This argues for a value of $J_{\rm ion,21}/J_{\rm 21,LW}$ that is lower than $\langle f_{\rm esc} \rangle$. Furthermore, the simulations by Gnedin et al. (2008) suggest that the escape fraction of ionizing photons varies significantly from sightline-to-sightline, with a small fraction of sightlines having $f_{\rm esc} = 1$, and a significant fraction having $f_{\rm esc} \lesssim 10^{-3}$ (mainly because of intervening H I and He I). This also implies that it is likely that $J_{\rm ion,21}/J_{\rm 21,LW} \lesssim \langle f_{\rm esc} \rangle$.

4.4 The transition from massive to supermassive black hole

Even if a 10^4–10^6 $M_\odot$ BH forms as a direct result of the collapse of a gas cloud that was irradiated by an LW flux that exceeded $J_{\rm crit}$, the BH still needs to grow to 10^9 $M_\odot$. This requires the BH to consume a tremendous amount of gas over ∼0.5 Gyr (the total time that elapsed between $z = 10$ and 6). This implies that the original host halo in which the BH formed, must merge with other haloes into a massive 10^{12}–10^{13} $M_\odot$ host halo (which also agrees with the mass of the host haloes of the $z \sim 6$ quasars; see e.g. the review by Haiman & Quataert 2004). Interestingly, we found that those $M = 10^8$ $M_\odot$ haloes that are exposed to an LW flux exceeding $J_{\rm crit}$, are the ones with a nearby star-forming galaxy. The halo mass of this nearby galaxy is possibly as large as 10^{11} $M_\odot$ (see Section 3.3), and the 10^4–10^6 $M_\odot$ BH is likely to end up inside this larger DM halo.

Utilizing Lacey & Cole (1993, equation 2.16), we find that the fraction of all 10^8 $M_\odot$ haloes at $z = 10$ that are incorporated into $M \geq 10^{12}$ $M_\odot$ haloes by $z = 6$ is 1.4×10^{-4}. This fraction is much larger (by a factor of $\sim 10^3$) than the fraction of haloes that have close and massive neighbours and are irradiated by a critical flux. This is strongly suggestive that essentially all of these strongly irradiated haloes are in the highly clustered tail of the spatial distribution, and will end up in massive haloes, such as those hosting the SDSS quasars, by $z = 6$. For reference, we also note that the 10^8 $M_\odot$ haloes contain a fraction 1.6×10^{-2} of the total mass at $z = 10$, while 10^{12} $M_\odot$ haloes at $z = 6$ have a mass fraction of 2.8×10^{-5} at $z = 6$. This implies that $\approx (1.6 \times 10^{-2}) \times (1.4 \times 10^{-4})/(2.8 \times 10^{-5}) \approx 10$ per cent of the masses of the 10^{12} $M_\odot$ haloes at $z = 6$ were already assembled into 10^8 $M_\odot$ haloes at $z = 10$. In this picture, the $z = 6$ SMBHs originally formed inside collapsing 10^8 $M_\odot$ satellite haloes of more massive star-forming galaxies.

4.5 Metal enrichment of $T_{\rm vir} > 10^4$ K haloes

While the above discussion shows that a non-negligible fraction of haloes may be kept H_2-free by a strong LW background, another possible effect that could invalidate the direct-collapse BH formation scenario is the presence of heavy elements in such haloes. Indeed, most high-redshift DM haloes with $T_{\rm vir} \sim 10^4$ K may be already enriched with at least trace amounts of metals and dust produced by prior star formation in their progenitors. Omukai et al. (2008) recently studied the thermal and chemical evolution of low-metallicity gas exposed to extremely strong UV radiation fields. They find that these metals and any accompanying dust can catastrophically lower the gas temperature, producing an effective equation-of-state index of $\gamma \equiv {\rm d}\ln p/{\rm d}\ln\rho \ll 1$, even in the presence of a UV background as strong as $J_{\rm LW} = 10^3$, which keeps H_2 photodissociated. They suggest that gas fragmentation may thus be inevitable above a critical metallicity, whose value is between $Z_{\rm cr} \approx 3 \times 10^{-4}\,Z_\odot$ (in the absence of dust) and as low as $Z_{\rm cr} \approx 5 \times 10^{-6}\,Z_\odot$ (with a dust-to-gas mass ratio of about 0.01 $Z/Z_\odot$, also see Omukai 2000; Bromm et al. 2001; Schneider et al. 2003). When the metallicity exceeds these critical values, dense clusters of low-mass stars may form at the halo nucleus. While relatively massive stars in such a cluster could then rapidly coalesce into a single more massive object (which may produce an intermediate-mass BH remnant with a mass up to $M \lesssim 10^2$–10^3 $M_\odot$), the formation of much BHs as massive as $M \lesssim 10^5$–10^6 $M_\odot$ by direct collapse is likely to require – in addition to being exposed to a large $J_{\rm crit}$ – that the halo gas is also essentially metal-free. Metal enrichment by the nearby star-forming galaxy (i.e. responsible for the large local LW flux), is not necessarily a problem, since the expelled metals most efficiently mix in the outer edge of the collapsing halo, while leaving the inner core pristine (Greif et al. 2007; Cen & Riquelme 2008).

Downloaded from https://academic.oup.com/mnras/article/391/4/1961/1747710 by Scuola Normale Superiore Biblioteca user on 12 December 2025

5 CONCLUSIONS

H_2 molecules can be photodissociated by UV radiation, either directly (by photons with energies $E > 14.7$ eV, if the molecules are exposed to ionizing radiation) or as a result of electronic excitation by LW photons with energies 11.2 eV $\lesssim E < E_{\rm H}$. In this paper we focused on this latter process, which operates even in gas that is self-shielded, and/or in gas that is shielded by a neutral IGM prior to the completion of reionization (see Haiman et al. 1997), from radiation at $E > E_{\rm H}$.

Photodissociation feedback possibly plays an important role in the formation of the SMBHs ($M_{\rm BH} \sim 10^9\,{\rm M}_\odot$) that existed at redshift $z > 6$, when the age of the Universe was <1 Gyr (e.g. Fan 2006). The reason for this is that this feedback mechanism can affect gas cooling and collapse into haloes that have $T_{\rm vir} > 10^4$ K (e.g. Oh & Haiman 2002). Without H_2 molecules, gas inside these haloes collapses nearly isothermally due to atomic cooling, with the temperature remaining as high as $T \sim 10^4$ K, which may strongly suppress the ability of gas to fragment into stellar mass objects (e.g. Oh & Haiman 2002). Instead of fragmenting, this gas could rapidly accrete on to a seed BH (Volonteri & Rees 2005), or collapse directly into a very massive ($M_{\rm BH} = 10^4$–$10^6\,{\rm M}_\odot$) BH (Bromm & Loeb 2003; Begelman et al. 2006; Spaans & Silk 2006), possibly with an intermediate state in the form of a very massive star (see Omukai et al. 2008, for a more complete review). If these 'direct-collapse BHs' indeed formed, then they would provide a head start that could help explain the presence of SMBHs with inferred masses of several $\times 10^9\,{\rm M}_\odot$ by $z \approx 6$.

Possibly the most stringent requirement for the direct-collapse BH model, is the intensity of the photodissociating background, which must exceed $J_{21,\rm LW} \geq J_{\rm crit} \sim 10^3$ (Bromm & Loeb 2003, where $J_{21,\rm LW}$ denotes the intensity in the LW background in units of 10^{-21} erg s^{-1} Hz^{-1} sr^{-1} cm^{-2}, evaluated at the Lyman limit). Since the mean free path of LW photons is large, the LW background is expected to be nearly uniform, and likely significantly lower than $J_{\rm crit}$ (Omukai et al. 2008). However, some variation in the LW flux that irradiates individual DM haloes is expected. For example, a DM halo with a nearby star-forming galaxy may 'see' an LW flux that exceeds the background by orders of magnitude.

In this paper, we have modelled this variation and we have computed the PDF of the LW flux, $J_{\rm LW}$, that irradiates a high-redshift DM halo at $z = 10$. The main differences from previous works that study the spatial variation of the UV background are that: (i) we include (1) the non-linear clustering of sources, using the non-linear bias formalism developed by Iliev et al. (2003), which describes the clustering of closely separated haloes particularly well; (2) Poisson fluctuations in the number of surrounding star-forming galaxies; (3) the probable existence of a dispersion in LW luminosity for a given halo mass. In the local universe the UV luminosity can vary by orders of magnitude for a given stellar mass (e.g. Schiminovich et al. 2007), and a similar variation of the UV luminosity may be expected for a given halo mass; (ii) we specialize to compute the PDF of the flux as seen by high-redshift DM haloes; (iii) we focus on the tail of the flux PDF and (iv) we discuss the significance of this tail for rapid high-redshift SMBH growth.

We found that >99 per cent of the DM haloes at $z = 10$ are illuminated by LW flux that is within a factor of 2 from the global background value (Fig. 2). However, a tiny fraction ($f_{\rm crit} = 10^{-8}$ to 10^{-6}) of DM haloes with virial temperatures exceeding $T_{\rm vir} = 10^4$ K may see an LW flux that is boosted to the level $J_{\rm crit} = 10^3$ that is required by the direct collapse BH model, due to nearby luminous neighbours. We demonstrated that this result is insensitive both to our assumed model parameters (Fig. 6), and to radiative transfer effects due to intervening atomic and molecular hydrogen gas (Section 4.1).

Depending on (i) the duration for which haloes are producing UV luminosity ($t_{\rm lum}$), (ii) the duration for which the irradiation is needed to avoid fragmentation ($t_{\rm frag}$) and (iii) the spread in formation times of haloes ($t_{\rm form}$), these rare halo pairs provide possible sites in which primordial gas clouds collapse directly into massive BHs ($M_{\rm BH} \approx 10^{4-6}\,{\rm M}_\odot$, see Section 4.2). In Section 4.4, we showed that these BHs are likely to end up in massive (10^{12}–$10^{13}\,{\rm M}_\odot$) host haloes (which also agrees with the mass of the host haloes of the $z \sim 6$ quasars; see e.g. the review by Haiman & Quataert 2004), in which they can grow to $10^9\,{\rm M}_\odot$ within ∼0.5 Gyr (the total time that elapsed between $z = 10$ and 6). It is interesting to stress that in this picture, the $z = 6$ SMBHs originally formed inside collapsing $10^8\,{\rm M}_\odot$ satellite haloes of more massive star-forming galaxies.

The fraction $f_{\rm crit} \sim 10^{-8}$ to 10^{-6} translates to ∼10–$10^3 \gtrsim 10^8\,{\rm M}_\odot$ haloes per comoving Gpc^3 volume. The gas inside one of these haloes needs to collapse directly into a massive BH, and subsequently grow to a $M_{\rm BH} = 10^9\,{\rm M}_\odot$ to explain observed space density of $z = 6$ luminous quasars. The actual number of SMBHs at $z = 6$ is higher by a factor of $1/\epsilon_{\rm QSO}$, where $\epsilon_{\rm QSO}$ denotes the fraction of Hubble time that $z = 6$ SMBHs are observable as luminous quasars. Assuming a quasar lifetime of ∼50 Myr (e.g. Martini 2004), we have $\epsilon_{\rm QSO} \sim 0.05$, and the number density of $z = 6$ SMBHs is ∼20 cGpc^{-3}, which we conclude is manageable with the direct-collapse BH scenarios.

ACKNOWLEDGMENTS

MD is supported by Harvard University funds. ZH acknowledges support by the Polányi Program of the Hungarian National Office of Technology. JSBW acknowledges the support of the ARC. Partial support for this work was also provided by NASA through Hubble Fellowship grant #HF-01222.01 to AM, awarded by the Space Telescope Science Institute, which is operated by the Association of Universities for Research in Astronomy, Inc., for NASA, under contract NAS 5-26555.

REFERENCES

Ahn K., Shapiro P. R., Iliev I. T., Mellema G., Pen U.-L., 2008, preprint (arXiv:0807.2254)
Barkana R., Loeb A., 2001, Phys. Rep., 349, 125
Begelman M. C., Volonteri M., Rees M. J., 2006, MNRAS, 370, 289
Bouwens R. J., Illingworth G. D., Blakeslee J. P., Franx M., 2006, ApJ, 653, 53
Bromley J. M., Somerville R. S., Fabian A. C., 2004, MNRAS, 350, 456
Bromm V., Loeb A., 2003, ApJ, 596, 34
Bromm V., Ferrara A., Coppi P. S., Larson R. B., 2001, MNRAS, 328, 969
Cen R., Riquelme M. A., 2008, ApJ, 674, 644
Chen H.-W., Prochaska J. X., Gnedin N. Y., 2007, ApJ, 667, L125
Couchman H. M. P., Rees M. J., 1986, MNRAS, 221, 53
Croft R. A. C., 2004, ApJ, 610, 642
Dijkstra M., Haiman Z., Rees M. J., Weinberg D. H., 2004, ApJ, 601, 666
Dijkstra M., Wyithe J. S. B., Haiman Z., 2007, MNRAS, 379, 253
Dunkley J. et al., 2008, ApJS, in press (arXiv.org:0803.0586)
Efstathiou G., 1992, MNRAS, 256, 43P
Fan X., 2006, New Astron. Rev., 50, 665
Fan X. et al., 2001, AJ, 122, 2833
Fan X. et al., 2003, AJ, 125, 1649
Gnedin N. Y., Kravtsov A. V., Chen H.-W., 2008, ApJ, 672, 765
Greif T. H., Johnson J. L., Bromm V., Klessen R. S., 2007, ApJ, 670, 1
Haiman Z., 2004, ApJ, 613, 36

Downloaded from https://academic.oup.com/mnras/article/391/4/1961/1747710 by Scuola Normale Superiore Biblioteca user on 12 December 2025

Haiman Z., Loeb A., 2001, ApJ, 552, 459
Haiman Z., Quataert E., 2004, ASSL, 308, 147
Haiman Z., Thoul A. A., Loeb A., 1996, ApJ, 464, 523
Haiman Z., Rees M. J., Loeb A., 1997, ApJ, 476, 458
Haiman Z., Abel T., Rees M. J., 2000, ApJ, 534, 11
Hennawi J. F. et al., 2006, AJ, 131, 1
Iliev I. T., Scannapieco E., Martel H., Shapiro P. R., 2003, MNRAS, 341, 81
Johnson J. L., Bromm V., 2007, MNRAS, 374, 1557
Johnson J. L., Greif T. H., Bromm V., 2007, ApJ, 665, 85
Johnson J. L., Greif T. H., Bromm V., 2008, MNRAS, 388, 26
Kennicutt R. C. Jr., 1998, ARA&A, 36, 189
Kitayama T., Ikeuchi S., 2000, ApJ, 529, 615
Komatsu E. et al., 2008, ApJS, in press (arXiv.org:0803.0547)
Kuhlen M., Madau P., 2005, MNRAS, 363, 1069
Lacey C., Cole S., 1993, MNRAS, 262, 627
Lee K., Giavalisco M., Conroy C., Wechsler R. H., Ferguson H. C., Somerville R. S., Dickinson M. E., Urry C. M., 2008, preprint (arXiv:0808.1727)
Lepp S., Shull J. M., 1984, ApJ, 280, 465
Li Y. et al., 2007, ApJ, 665, 187
Lodato G., Natarajan P., 2006, MNRAS, 371, 1813
Lodato G., Natarajan P., 2007, MNRAS, 377, L64
Martini P., 2004, in Ho L. C., ed., Carnegie Observatories Astrophysics Series, Vol. 1, Coevolution of Black Holes and Galaxies. Cambridge Univ. Press, Cambridge, p. 169
Mesinger A., Bryan G. L., Haiman Z., 2006, ApJ, 648, 835
Meiksin A., White M., 2004, MNRAS, 350, 1107
Mesinger A., Dijkstra M., 2008, MNRAS, 390, 1071
Mesinger A., Furlanetto S., 2007, ApJ, 669, 663
Mesinger A., Furlanetto S. R., 2008, MNRAS, 386, 1990
Mo H. J., White S. D. M., 1996, MNRAS, 282, 347
Oh S. P., Haiman Z., 2002, ApJ, 569, 558
Omukai K., 2000, ApJ, 534, 809
Omukai K., Schneider R., Haiman Z., 2008, ApJ, 686, 801
Press W. H., Schechter P., 1974, ApJ, 187, 425
Ricotti M., Gnedin N. Y., Shull J. M., 2001, ApJ, 560, 580
Saslaw W. C., Zipoy D., 1967, Nat, 216, 976
Scannapieco E., Barkana R., 2002, ApJ, 571, 585
Schaye J., 2006, ApJ, 643, 59
Schiminovich D. et al., 2007, ApJS, 173, 315
Schneider R., Ferrara A., Salvaterra R., Omukai K., Bromm V., 2003, Nat, 422, 869
Shapiro S. L., 2005, ApJ, 620, 59
Shapiro P. R., Kang H., 1987, ApJ, 318, 32
Shapley A. E., Steidel C. C., Pettini M., Adelberger K. L., Erb D. K., 2006, ApJ, 651, 688
Sheth R. K., Mo H. J., Tormen G., 2001, MNRAS, 323, 1
Siana B. et al., 2007, ApJ, 668, 62
Spaans M., Silk J., 2006, ApJ, 652, 902
Stark D. P., Ellis R. S., Richard J., Kneib J.-P., Smith G. P., Santos M. R., 2007, ApJ, 663, 10
Tanaka T., Haiman Z., 2008, ApJ, submitted (arXiv:0807.4702)
Thoul A. A., Weinberg D. H., 1995, ApJ, 442, 480
Thoul A. A., Weinberg D. H., 1996, ApJ, 465, 608
Volonteri M., Rees M. J., 2005, ApJ, 633, 624
Volonteri M., Rees M. J., 2006, ApJ, 650, 669
Volonteri M., Lodato G., Natarajan P., 2008, MNRAS, 383, 1079
Whalen D., Abel T., Norman M. L., 2004, ApJ, 610, 14
Woosley S. E., Bloom J. S., 2006, ARA&A, 44, 507
Wyithe J. S. B., Loeb A., 2006, Nat, 441, 322
Yoo J., Miralda-Escudé J., 2004, ApJ, 614, 25
Zuo L., 1992, MNRAS, 258, 36

This paper has been typeset from a TEX/LATEX file prepared by the author.

Downloaded from https://academic.oup.com/mnras/article/391/4/1961/1747710 by Scuola Normale Superiore Biblioteca user on 12 December 2025